Uncertainty Maps in Dynamic Contrast-Enhanced MRI

Anders Garpebring[1], Patrik Brynolfsson[1], Jun Yu[2], Ronnie Wirestam[3], Adam Johansson[1], Thomas Asklund[4], and Mikael Karlsson[1]
[1]*Dept. of Radiation Sciences, Umeå University, Umeå, Sweden,* [2]*Centre of Biostatistics, Swedish University of Agricultural Sciences, Umeå, Sweden,* [3]*Dept. of Medical Radiation Physics, Lund University, Lund,* [4]*Division of Oncology, Dept. of Radiation Sciences, Umeå University, Umeå, Sweden*

Introduction

In dynamic contrast-enhanced (DCE) MRI, errors propagate in a highly non-trivial way from a number of sources of uncertainty to the parametric maps. Several authors have investigated this topic using simulations, *e.g.*, Kershaw *et al.* [1]. However, knowledge of the uncertainty should, ideally, accompany each parametric map in DCE-MRI. For this purpose, explicit equations for the uncertainty are preferred since they do not require time-consuming multiple refitting of models to the data. The aim of this work was to develop and investigate a linear multivariate error propagation method applicable to number of different and complex sources of uncertainty.

Method

Ideally, at sufficient SNR, magnitude MR images show normally distributed and temporally uncorrelated noise over the image series collected in a DCE-MRI experiment. Thus, it is optimal [2] to use the ordinary least squares (OLS) estimator to find the pharmacokinetic (PK) parameters $\mathbf{p}$. However, a combined signal and pharmacokinetic model, f, depends on other parameters than $\mathbf{p}$, *e.g.*, the arterial input function (AIF), baseline signal (S_0), baseline T_1 (T_{10}), contrast agent relaxivity, flip angle, etc., and all of these are associated with a given uncertainty. Let these parameters be denoted $\hat{\mathbf{q}}$ and let the measured values of the time curve in a voxel be S_i. The OLS estimate $\hat{\mathbf{p}}$ of $\mathbf{p}$ is then given by

$$\hat{\mathbf{p}} = \arg\min_{\mathbf{p}} \sum_i \left(S_i - f\left(t_i, \mathbf{p}, \hat{\mathbf{q}}\right)\right)^2, \qquad (1)$$

where t_i denotes sampling time-points. A linear approximation can be used to find for the covariance of $\hat{\mathbf{p}}$ if the noise in $\hat{\mathbf{p}}$ and $\hat{\mathbf{q}}$ are sufficiently small and if the noise in S_i and $\hat{\mathbf{q}}$ are independent. The covariance is given by

$$\mathrm{cov}\left(\hat{\mathbf{p}}\right) \approx \left(\hat{\mathbf{J}}_{\mathbf{p}}^T \hat{\mathbf{J}}_{\mathbf{p}}\right)^{-1} \hat{\sigma}_s^2 + \hat{\mathbf{J}}_{\mathbf{p}}^- \hat{\mathbf{J}}_{\mathbf{q}}\, \mathrm{cov}\left(\hat{\mathbf{q}}\right) \left(\hat{\mathbf{J}}_{\mathbf{p}}^- \hat{\mathbf{J}}_{\mathbf{q}}\right)^T, \qquad (2)$$

where $\hat{\sigma}_S^2$ is an estimate of the variance of the noise in the signal S_i, $\hat{\mathbf{J}}_{\mathbf{p}}^- = \left(\hat{\mathbf{J}}_{\mathbf{p}}^T \hat{\mathbf{J}}_{\mathbf{p}}\right)^{-1} \hat{\mathbf{J}}_{\mathbf{p}}^T$, $\hat{\mathbf{J}}_{\mathbf{p},ij} = \partial f\left(t_i, \hat{\mathbf{p}}, \hat{\mathbf{q}}\right) / \partial \hat{p}_j$ and $\hat{\mathbf{J}}_{\mathbf{q},ij} = \partial f\left(t_i, \hat{\mathbf{p}}, \hat{\mathbf{q}}\right) / \partial \hat{q}_j$. Equation (2) was compared with Monte Carlo simulated uncertainties for the spoiled gradient echo sequence and the extended Tofts model [3]. Settings used in the simulation were TR/TE = 4/1.79 ms, flip angle = 20°, total duration/temporal resolution = 424/2.65 s, the transfer constant K^{trans} = 0.15 min^{-1}, extracellular extravascular volume fraction v_e = 0.30, and the blood plasma volume fraction v_p = 0.04. Four different sources of uncertainty were investigated by adding noise to S_i, S_0, T_{10}, and by introducing a random error in the AIF peak and tail amplitudes. All noise sources were normally distributed with zero mean. The two variables that introduced errors in the AIF were independent. In the Monte Carlo simulation, 10 000 repeated fits, at each noise level, were performed to find the simulated coefficient of variation (CV) of $\hat{\mathbf{p}}$. For each simulation, Eq. (2) was evaluated to yield an estimated CV of $\hat{\mathbf{p}}$. When evaluating Eq. (2), $\hat{\sigma}_S^2$ was found from the residuals of the fit, while the true covariances of the AIF, S_0 and T_{10} were used. The proposed method was also tested on real data, acquired with the same imaging settings as in the simulation. The variances of S_0 and T_{10} were found from 20 baseline images and the standard error from the calculation of T_{10}. The covariance of the AIF was extracted from 10 measured AIFs.

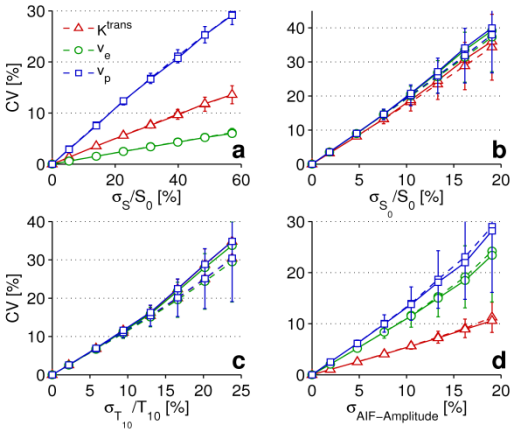

Figure 1: Solid line represents Monte Carlo simulated CV and dashed line is estimated CV using Eq. (2). The error bars represent one standard deviation in estimated CV. CV of PK parameters due to noise in S_i (**a**), noise in S_0 (**b**), noise in T_{10} (**c**), and errors in the AIF amplitude (**d**).

Results

Figure 1 shows the results of the Monte Carlo simulation and the uncertainty estimation. The agreement was in general good but at high noise levels deviations are apparent especially for noise in the baseline signal (**b**) and in the baseline T_{10} value (**c**). Furthermore, the precision tended to deteriorate at high noise levels. Figure 2 (**a**) and (**b**) show a K^{trans} map and a map of the standard deviation in K^{trans}, respectively. In Figure 2 (**c**) and (**d**), the CVs of K^{trans}, v_e, and v_p in the two pixels indicated in (**a**) are displayed.

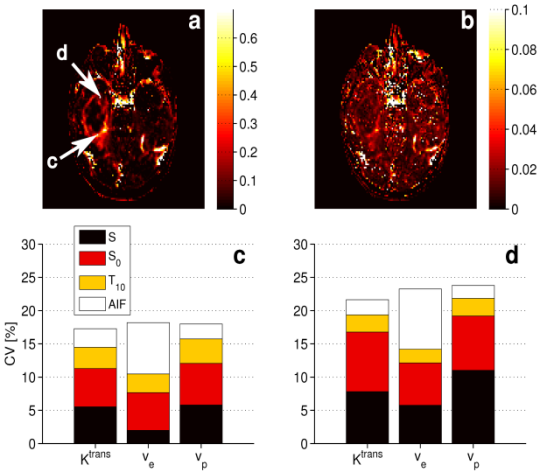

Figure 2: (**a**) K^{trans} map. (**b**) Map of standard deviation of K^{trans}. (**c**) CV of a voxel indicated in (**a**). (**d**) CV of a voxel indicated in (**a**). The CVs in (**c**) and (**d**) are subdivided to show the contributions from each source of uncertainty to the total variance.

Discussion and conclusions

The Monte Carlo simulations indicate that Eq. (2) accurately predicts the CV of the estimated parameters at moderate noise levels also for complicated sources of uncertainty such as the AIF. That Eq. (2) is limited to moderate noise was expected from the linear approximation. The example on real data shown in Figure 2 demonstrates that spatially resolved maps of uncertainty subdivided by origin are feasible *in vivo*.

[1] Kershaw, L. E., Cheng, H.-L. M. *Magnetic Resonance in Medicine* 2010, 64, 1772-80.
[2] Seber, G. A. F., Wild, C. J. Nonlinear regression; Wiley: New York, 1989.
[3] Tofts, P. S. *Journal of Magnetic Resonance Imaging* 1997, 7, 91-101.